HAL
open science

Unshielded Cable modeling for Conducted Emissions Issues in Electrical Power Drive Systems

Victor dos Santos, Nicolas Roux, Bertrand Revol, Bruno Sareni, Bernardo Cougo, Jean-Pierre Carayon

To cite this version:

Victor dos Santos, Nicolas Roux, Bertrand Revol, Bruno Sareni, Bernardo Cougo, et al.. Unshielded Cable modeling for Conducted Emissions Issues in Electrical Power Drive Systems. 2017 International Symposium on Electromagnetic Compatibility (EMC EUROPE), Sep 2017, Angers, France. pp. 1-6. hal-01656080

HAL Id: hal-01656080

https://hal.science/hal-01656080v1

Submitted on 5 Dec 2017

HAL is a multi-disciplinary open access archive for the deposit and dissemination of scientific research documents, whether they are published or not. The documents may come from teaching and research institutions in France or abroad, or from public or private research centers.

L'archive ouverte pluridisciplinaire **HAL**, est destinée au dépôt et à la diffusion de documents scientifiques de niveau recherche, publiés ou non, émanant des établissements d'enseignement et de recherche français ou étrangers, des laboratoires publics ou privés.

Open Archive TOULOUSE Archive Ouverte (OATAO)
OATAO is an open access repository that collects the work of Toulouse researchers and makes it freely available over the web where possible.

This is an author-deposited version published in : http://oatao.univ-toulouse.fr/
Eprints ID : 18265

To link to this article : DOI: 10.1109/EMCEurope.2017.8094736
URL : http://dx.doi.org/10.1109/EMCEurope.2017.8094736

To cite this version : Dos Santos, Victor and Roux, Nicolas and Revol, Bertrand and Sareni, Bruno and Cougo, Bernardo and Carayon, Jean-Pierre *Unshielded Cable modeling for Conducted Emissions Issues in Electrical Power Drive Systems.* (2017) In: EMC Europe 2017, 4 September 2017 - 8 September 2017 (Angers, France).

Any correspondence concerning this service should be sent to the repository administrator: staff-oatao@listes-diff.inp-toulouse.fr

Unshielded Cable Modeling for Conducted Emissions Issues in Electrical Power Drive Systems

Victor Dos Santos[1,2], Nicolas Roux[2], Bertrand Revol[3], Bruno Sareni[2], Bernardo Cougo[1], Jean-Pierre Carayon[1]
[1] IRT Saint Exupéry, 118 route de Narbonne, 31432 Toulouse cedex 4, France
Email : victor.dossantos@irt-saintexupery.com
[2] Université de Toulouse, LAPLACE, UMR CNRS-INP-UPS, 2 rue Charles Camichel, 31071 Toulouse cedex, France
Email: nicolas.roux@laplace.univ-tlse.fr - bruno.sareni@laplace.univ-tlse.fr
[3] SATIE – ENS Paris Saclay, 61 avenue du Président Wilson, 94235 Cachan cedex, France
Email: bertrand.revol@satie.ens-cachan.fr

***Abstract*—In power electronics applications, high frequency models for cables are necessary to understand EMI issues in pulsewidth modulation drives. This paper shows the approach developed at the French Institute of Technology (IRT) Saint-Exupery, in order to take account of the frequency dependency of unshielded power cables per-unit-length parameters for EMC simulations. Fast, predictive models are compared to different shapes numerical models. The method was applied to unshielded two and three wires cables. Finally, common mode (CM) emissions modeling is proposed to predict the CM noise currents, which are the most disturbing in any variable-speed drive systems. The modeling principle is to consider the complete CM circuit as a chain of quadripolar matrices.**

Keywords—Cable; Unshielded cable; Drive; EMI; Conducted emissions; Common mode; Modeling; High Frequency.

ACRONYMS LIST

Acronym	Parameter
J	Current density
f	Frequency
r, l, c	Per unit length resistance, inductance, capacitance
$\boldsymbol{\mu_0}$	Magnetic permeability, $\boldsymbol{\mu_0 = 4\pi.10^{-7}\ H.m^{-1}}$
$\boldsymbol{\mu_r}$	Relative permeability
$\boldsymbol{\epsilon_0}$	Vacuum permittivity, $\epsilon_0 = 10^{-9}/(36.\pi)\ F.m^{-1}$
$\boldsymbol{\epsilon_r}$	Relative permittivity
$\boldsymbol{\rho}$	Resistivity of conductor material
$\boldsymbol{q}$	Charge per unit [C/m]
r	Conductor radius
$\boldsymbol{h_{i0}}$	Distance between the wire and the ground plane
$\boldsymbol{d_{ij}}$	Distance between conductor n°i and n°j
$\boldsymbol{D_{ij}}$	Distance between conductor n°i and image of n°j

I. INTRODUCTION

As it can be seen in literature, in the last decades, the high frequency behavior of power cables in Pulse Width Modulation (PWM) motor drives has become a high-priority topic in the analysis of transient overvoltages and conducted electromagnetic interference (EMI) propagation, both common and differential mode. According to the actual power electronics trends, the development of new Wide Bandgap (WBG) semiconductor technologies (transistors and diodes), can significantly increase efficiency, performance and power density of adjustable speed electrical power drive systems. These components, made of Gallium Nitride (GaN) or Silicon Carbide (SiC) offer faster switching speeds, low losses, and the ability to function at high operating temperatures compared to their silicon counterparts. Nevertheless, the higher switching speeds (dv/dt) in modern PWM motor drives are mainly responsible for fast currents and voltages transients that lead to serious EMC issues from conducted and radiated EMI.

Such modeling also fosters a better understanding of physical phenomena such the overvoltages in drive systems. Overvoltages are the results of propagation and reflection phenomena along the harness, up to twice the DC link voltage at the motor terminals. In this paper, the Multi Transmissions Line theory is reminded, first. Then, analytical and numerical models are presented for the case of unshielded two and three wires cables. Lastly, some parametric studies are carried out to illustrate the need of predictive and high frequency cables models in common mode emissions studies.

II. ELECTRICAL POWER DRIVE SYSTEM DESCRIPTION

The studied system is a variable speed electrical power drive system. Fig 1 provides a schematic overview of the studied system. It is composed of two Line Impedance Stabilization Networks (LISN), a three-phase SiC MOSFET inverter, an aeronautical Permanent Magnet Synchronous Motor (PMSM) and two non-shielded aeronautical cables: one links up the LISN and the inverter (two conductors, one meter length) and another connects the inverter to the motor (three conductors). The electromechanical drive will be situated on a 6 m² copper plane, excluding a loaded induction generator used as the load of the system placed over insulation foams to insulate them from the ground. The complete system is placed in a Faraday cage.

The cable used in this study is an aeronautical cables from Draka manufacturer (DM Series AWG8 EN 2267-008A090P). Dimensions and physical parameters are defined in EN 2267-008 standard. Key figures are provided in Table I.

Electromagnetic disturbances have to be compliant with the EMI standard, here the commercial aircraft standard DO-160G [1]. Regarding power cables integration, the normative setup stipulates that the cable layout has to be 5 cm above the ground plane.

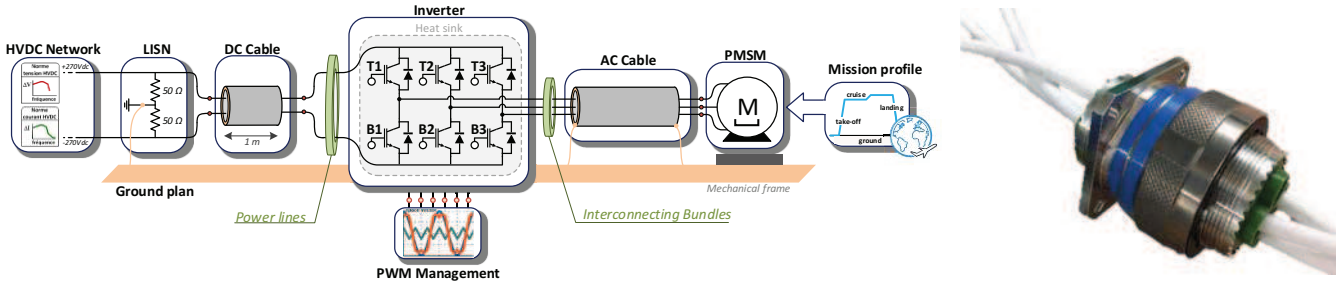

Fig. 1. Electromechanical Drive in the normative conditions according to the DO-160 Standard & Aeronautic connectors and cables

III. Multiconductor Transmission Line Theory

Since the early days of telegraph, parallel conductors were used to guide electrical signals from one point to another. Therefore, the Transmission Line (TL) model has been studied, used and analyzed through numerous fields of electrical engineering. Prof. C. R. Paul has presented a systematic approach and a unitary view of the TL model and to its generalization, the Multiconductor Transmission Line (MTL) model [2]. Starting from the general properties of the transverse electromagnetic (TEM) mode of propagation, he derived the TL equations using several approaches integrating integral equation techniques, matrix algebra and properties of the linear and nonlinear systems applied to electromagnetic theory. He provided the derivation of the MTL equations along with the general properties of the per-unit-length parameters in those equations.

$$\frac{\partial}{\partial z}\boldsymbol{V}(z,t) = -\boldsymbol{R}.\boldsymbol{I}(z,t) - \boldsymbol{L}.\frac{\partial}{\partial z}\boldsymbol{I}(z,t) \tag{1}$$

$$\frac{\partial}{\partial z}\boldsymbol{I}(z,t) = -\boldsymbol{G}.\boldsymbol{V}(z,t) - \boldsymbol{G}.\frac{\partial}{\partial z}\boldsymbol{V}(z,t) \tag{2}$$

The line parameters are obtained depending on the geometry of the line configuration. These parameters are extracted per line unit length. The series resistance of the line originates from the ohmic resistance of the metallic conductor. The series inductance and the shunt capacitance result from the effects of magnetic and electric fields induced by the voltage and current. The shunt conductance is due to the leakage currents occurring in the insulators and in the insulating medium. The shunt currents are normally very small, wherewith the shunt conductance is often neglected.

With the MTL approach, the per unit length matrices $\boldsymbol{R}$ and $\boldsymbol{L}$ are symmetric as shown in (3) and (4). The per unit length capacitance matrix $\boldsymbol{C}$ represents the displacement current flowing between the conductors in the transverse plane and is defined from (5).

$$\boldsymbol{R} = \begin{bmatrix} r_0 + r_1 & r_0 & \cdots & r_0 \\ r_0 & r_0 + r_2 & \cdots & r_0 \\ \vdots & \vdots & \ddots & \vdots \\ r_0 & r_0 & \cdots & r_0 + r_N \end{bmatrix} \tag{3}$$

$$\boldsymbol{L} = \begin{bmatrix} l_{11} & l_{12} & \cdots & l_{1N} \\ l_{21} & l_{22} & \cdots & l_{2N} \\ \vdots & \vdots & \ddots & \vdots \\ l_{N1} & l_{N2} & \cdots & l_{NN} \end{bmatrix} \tag{4}$$

$$\boldsymbol{C} = \begin{bmatrix} \sum_{k=1}^{N} c_{1k} & -c_{12} & \cdots & -c_{1N} \\ -c_{21} & \sum_{k=1}^{N} c_{2k} & \cdots & -c_{2N} \\ \vdots & \vdots & \ddots & \vdots \\ -c_{N1} & -c_{N2} & \cdots & \sum_{k=1}^{N} c_{Nk} \end{bmatrix} \tag{5}$$

The evolution of the linear parameters of the cable as a function of the temperature is neglected in this study. Indeed, the cable gauge has been sized according with a number of aeronautical standards criteria; among which are short circuit current constraint and the wire skin temperature limitations. Thus, given the current levels of application and the gauge chosen, it is justified to assume that the resistivity of the driver does not fluctuate too much.

The aim now is to find formulae for the line parameters, or extract them with the use of numerical approaches.

TABLE I. Geometrical Cable Specifications

Wire		
Parameter	***Unit***	***Value***
No of strands	-	127
Strand diameter	mm	0.30
Conductor diameter (max)		4.2
Wire diameter (min)		4.47
Wire diameter (max)		4.77

Insulation		
Parameter	***Unit***	***Value***
Fluorocarbon	µm	2.5
Polyimide		30
Fluorocarbon		2.5
PTFE – First tape		100
PTFE – Second tape		65

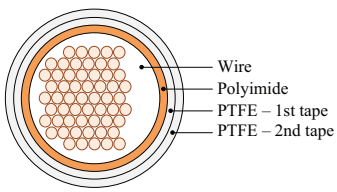

IV. Unshielded Two-Phase Cable Models

It is customary to model the operation of two-wire cables by a distributed constant circuit [2], [3]. The line is thus considered to be homogeneous. The equivalent circuit of a uniformly distributed constant-line portion is shown in Fig 2.

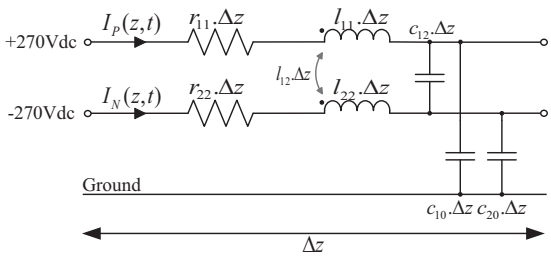

Fig. 2. Classical lumped circuit for a two-phase unshielded cable

A. Analytical Models

1) Per-Unit-Length Resistance

With increasing frequency, as is well known, the electric current flows mainly at the skin of the conductor, between the outer surface and the skin depth δ. The skin effect causes the effective resistance of the conductor to increase at higher frequencies where the skin depth is smaller. The resistance parameter of per-unit-length conductor is defined in (6).

$$r_{ii} = \frac{\rho}{S} = \rho.\frac{1}{\pi[r^2-(r-\delta)^2]} \quad \text{with,} \quad \delta = \frac{1}{\sqrt{\pi\mu\sigma f}} \tag{6}$$

2) Per-Unit-Length Inductance

Inner Inductance – For the derivation of the inner inductance we first compute the magnetic energy within one length unit of the conductor:

$$W_{in} = \frac{\mu_r\mu_0}{2}\int_V H_{in}^2 dV = \frac{\mu_r\mu_0}{2}\int_0^r \left(\frac{xI}{2\pi r^2}\right)^2 2\pi x dx \tag{7}$$

The inner inductance is equal to

$$l_{in} = \frac{W_{in}}{I^2} = \frac{\mu_r\mu_0}{8\pi} \tag{8}$$

Since the skin effect causes a current at high frequencies to flow mainly at the surface of a conductor, it can be seen [4] [5] that this will reduce the magnetic field inside the wire, modifying the inner inductance (9).

$$l_{in} = \frac{\mu_0}{8\pi}.\frac{10^{-3}}{r'}\sqrt{\frac{\mu_r}{\sigma f}} \quad \text{with} \quad r' = r.\sqrt{1-\left(\frac{2r}{d_{ij}}\right)^2} \tag{9}$$

Outer Inductance – For determining the part of the inductance originating by the field outside the conductor we consider the magnetic flux from the conductor surface within a radius x, as described in Fig. 3(b):

$$l_{out} = \frac{\mu_0}{\pi}\ln\left(\frac{2h_{i0}-r}{r}\right) \tag{10}$$

$$l_{ii} = l_{in} + l_{out} = \frac{\mu_0}{\pi}\left(\frac{10^{-3}}{8.r'}\sqrt{\frac{\mu_r}{\sigma f}} + \ln\left(\frac{2h_{i0}-r}{r}\right)\right) \tag{11}$$

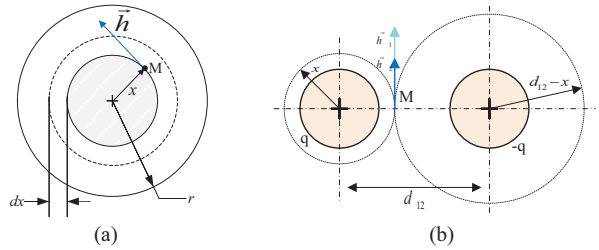

Fig. 3. Inductances extraction : (a) Inner, (b) Outer.

Mutual Inductance – .By the method of images, we may replace the plane with the cable image located at an equal distance h_{i0} below the position of the plane The mutual coupling between wires can be thus expressed as :

$$l_{ij} \cong \frac{\mu_0}{2\pi}\ln\left(\frac{D_{ij}}{d_{ij}}\right) \cong \frac{\mu_0}{2\pi}\ln\left(\sqrt{d_{ij}^2+4.h_{i0}^2}/d_{ij}\right) \tag{12}$$

3) Per-Unit-Length Capacitance

Wire to Wire Capacitance – Consider the two wires carrying charge uniformly distributed around each wire periphery as shown in Fig 4(a). The electric field assessed in M point is,

$$E_x = e_1 + e_2 = \frac{q}{2\pi\epsilon_0\epsilon_r}\left(\frac{1}{x}+\frac{1}{d_{ij}-x}\right) \tag{13}$$

Then, the voltage between the wires can similarly be obtained by superimposing the voltages due to the two equal but opposite charge distributions as defined in (14).

$$v = \int_r^{d_{ij}-r} E_x dx = \frac{q}{2\pi\epsilon_0\epsilon_r}\left[\int_r^{d_{ij}-r}\frac{dx}{x} + \int_r^{d_{ij}-r}\frac{dx}{d_{ij}-x}\right] \tag{14}$$

The per-unit-length capacitance is

$$c_{ij} = \frac{q}{v} = \frac{\pi.\varepsilon_0.\varepsilon_r}{ln\left(\frac{d_{ij}-r}{r}\right)} \tag{15}$$

Ground Capacitance – In order to calculate the capacitive coupling between the feeders and the ground plane, we consider the case of one wire at a height h above and parallel to an infinite, perfectly conducting plane. By the method of images, this problem can be related to the problem of the previous sub-section, as shown in Fig 4(b). Ground capacitance is equal to :

$$c_{i0} = 2.c_{two-wire} = \frac{2\pi\varepsilon_0\varepsilon_r}{\cosh^{-1}\left(\frac{h_{i0}}{r}\right)} \cong \frac{2\pi\varepsilon_0\varepsilon_r}{ln\left(\frac{2h_{i0}}{r}\right)} \tag{16}$$

Where,

$$\cosh^{-1}(h_{i0}/r) \cong \ln(2h_{i0}/r) \text{ because } r \ll h_{i0}.$$

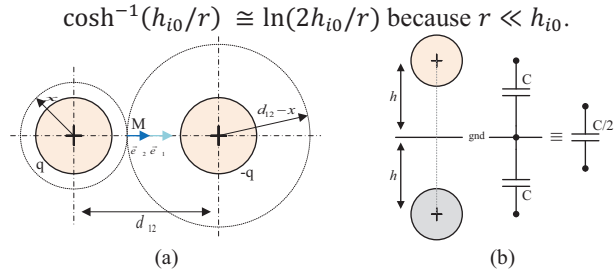

Fig. 4. Capacitance extraction : (a) Wire to wire, (b) Wire to ground plane.

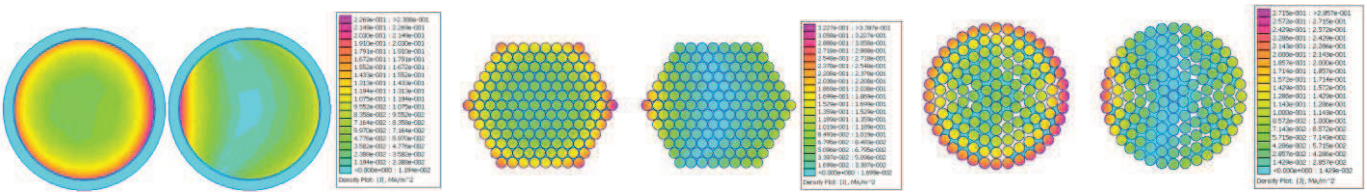

a) b) c)

Fig. 5. Current density in a two-phase non-shielded cable models (f = 20 kHz, $I_1 = 1\ A$, $I_2 = 0\ A$)

B. Numerical Models

The second method used to determine the cable parameters consists of using an electromagnetic solver tool. This method makes it possible to determine inductance, resistance and capacitance between the cable conductors. In this study, the finite element code "FEMM" software was used [6]. Three numerical models have been developed, the first identifies as "no strands" shown Fig. 5(a), the second one with a trapezoidal shape Fig. 5(b). Finally, the most representative model is shown in Fig. 5(c), in which the strands are orderly placed on concentric layers.

C. Model comparison

Per-unit-length parameters evaluations are provided in Fig. 6 (one cable 5 cm above ground plane), Fig. 7 (two-phase cable 5 cm above ground plane) and table II.

There is a substantial match of the models up to a limit frequency of 30 MHz. However, the difference observed between the analytical model and the numerical ones, from 100 kHz to 100 MHz, is due to the fact that the proximity effect is not taken into account in the mathematical model. Introducing a frequency dependent corrector factor to adjust the analytical model could be one way for better results agreement.

From 30 MHz, a deflection can be noticed on the numerical model without strands compared to the other numerical models. It is explained by the non-consideration of the skin and proximity effects between the strands. This difference may also be due to a lack of mesh precision at the edge of the conductor, where the skin effect is located.

TABLE II. CAPACITANCES VALUES

	Analytical	Numerical
Wire to wire: c_{ij} [pF/m]	68.46	62.95
Wire to ground: c_{i0} [pF/m]	14.2	7.44

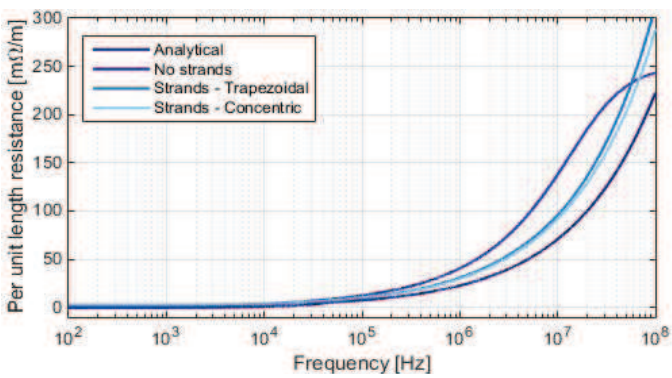

Fig. 6. Evolution of the per-unit-length resistance depending on frequency

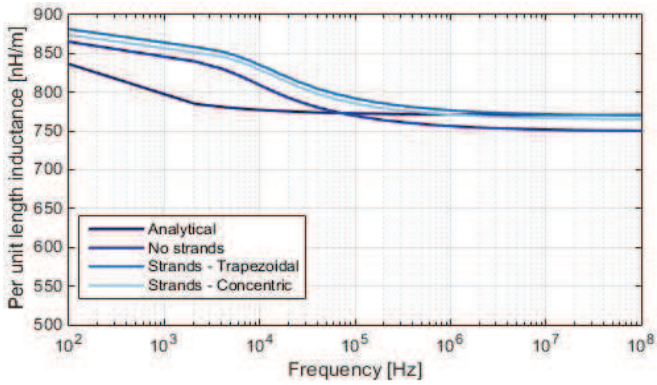

Fig. 7. Evolution of the per-unit-length inductance depending on frequency

V. UNSHIELDED THREE-PHASE CABLE MODELS

The previous case can be extended for a three phase cable. Fig. 8 show the classical lumped circuit for the three phase unshielded cable.

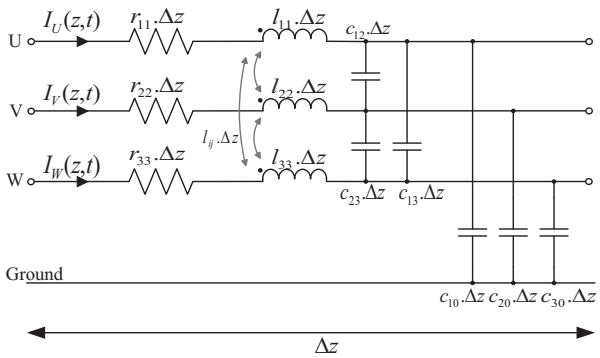

Fig. 8. Classical lumped circuit for a three-phase unshielded cable

A. Analytical Models

The per unit length parameters analytical expressions obtained in the previous section can also be extended to the three-phase case. Consequently, the line parameters for a three phase cable are listed in (17) to (21).

Per-unit-length resistance

$$r_{ii} = \frac{\rho}{S} = \rho.\frac{1}{\pi[r^2 - (r-\delta)^2]} \tag{17}$$

Per-unit-length inductance

$$l_{ii} \cong \frac{\mu_0}{\pi}\left(\frac{10^{-3}}{8.r'}\sqrt{\frac{\mu_r}{\sigma f}} + \ln\left(\frac{2h_{i0} - r}{r}\right)\right) \tag{18}$$

$$l_{ij} \cong \frac{\mu_0}{2\pi}\ln\left(\frac{D_{ij}}{d_{ij}}\right) \tag{19}$$

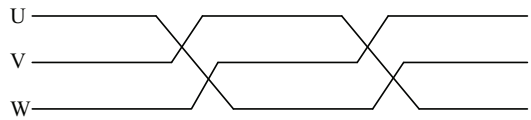

Fig. 9. Transposition in a three-wire cable

Per-unit-length capacitance A three phase line and the ground plane do not constitute a symmetrical system. To catch up the dissymmetry effects, a transposition is made in accordance with Fig. 9. Mathematical formulation of such transposition results in a change of the height of transmission lines formula (20).

$$c_{ij} \cong \frac{2\pi\varepsilon_0\varepsilon_r}{ln\left(\frac{h'}{r}\right)} \qquad \text{where,} \quad h' = \sqrt[3]{h_{10}h_{20}h_{30}} \tag{20}$$

$$c_{i0} = \frac{2\pi\varepsilon_0\varepsilon_r}{\cosh^{-1}\left(\frac{h'}{r}\right)} \cong \frac{2\pi\varepsilon_0\varepsilon_r}{ln\left(\frac{2h'}{r}\right)} \tag{21}$$

B. Numerical Models

AC cable can be viewed as a three conductor transmission line guided by transmission line theory. Fig. 10 shows the three numerical models previously developed extended to the three conductors case.

C. Model comparison

Fig. 11 and Fig. 12 show the longitudinal per-unit-length parameters varying with the AC current frequency.

Thanks to these graphs, the impact of the conductors modeling form on the evolution of the primary parameters of the cable as a function of the frequency is evaluated. Indeed, from 1 MHz, there is a noticeable difference between the models on the resistive part of the cable. For the inductive part, the shape impacts the entire frequency range.

TABLE III. COMPUTATIONAL TIME COST

Models	*Unit*	*Two-phase*	*Three-phase*
No strands	min	7.52	13.4
Trapezoidal		431.9	1003
Concentric		407.2	954.9

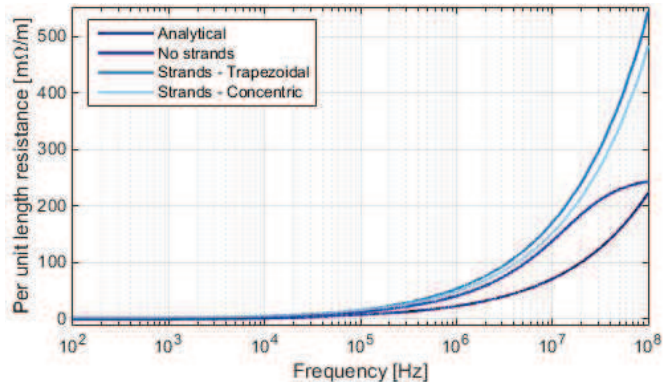

Fig. 11. Evolution of the per-unit-length resistance depending on frequency

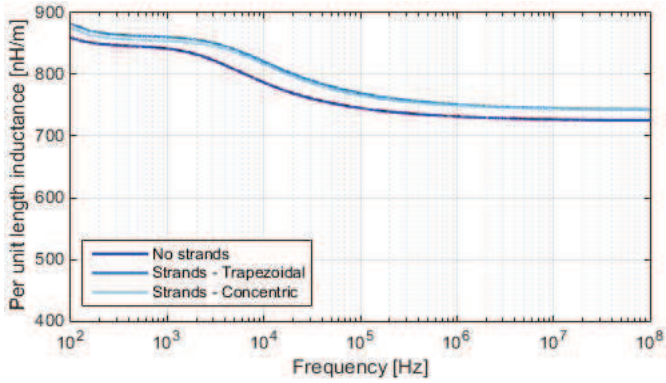

Fig. 12. Evolution of the per-unit-length inductance depending on frequency

Unfortunately, like any mesh associated with the physical description of an object, the more it is dense the longer the computation time cost is, as seen in Table III.

Authors in [7] proposed a cable model compatible with the Multiconductor Transmission Lines formalism. The used approach is less costly in terms of time consumption and IT resources. To avoid the problem of a too dense mesh, while retaining an interesting precision with respect to skin and proximity effects, they proposed a non-regular mesh with concentric layers of conductors of decreasing thickness at the periphery of the conductors.

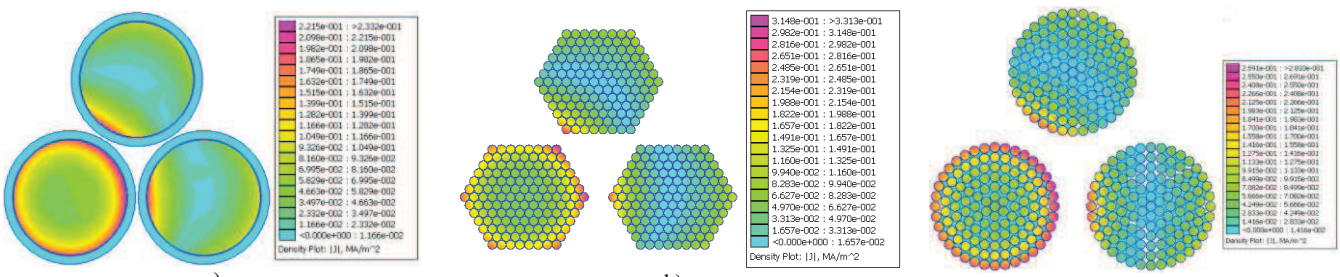

a) b) c)

Fig. 10. Current density in a three-phase non-shielded cable (f = 20 kHz, $I_U = 1\ A$, $I_V = I_W = 0\ A$)

VI. Conducted Emissions Modeling in Frequency Domain

Conducted emissions modeling of such system requires considering parasitic couplings in converters, feeding cables and motor windings. A fast method for CM emissions modeling is explained in [8]. The idea is to represent the CM equivalent circuit as a chain of two-port networks corresponding to each component of the system, see Fig. 13. The modeling principle is based on the hypothesis that the CM currents are mainly due to CM voltage.

The model is represented by a chain of two-port networks associated with impedance matrix $\boldsymbol{Z}$, which is then transformed into transfer matrix $\boldsymbol{T}$ in order to easily compute the equivalent matrix of the consecutive two-port networks in cascade. Therefore, the relation between the matrices $\boldsymbol{T}$ and $\boldsymbol{Z}$ has to be established.

The coefficients of matrix $\boldsymbol{Z}$ are defined by

$$[Z] = \begin{bmatrix} Z_{11} = V_1/I_1)_{I_2=0} & Z_{12} = V_1/I_2)_{I_1=0} \\ Z_{21} = V_2/I_1)_{I_2=0} & Z_{22} = V_2/I_2)_{I_1=0} \end{bmatrix} \quad (22)$$

The matrix $\boldsymbol{T}$ is defined by

$$[T] = \begin{bmatrix} T_{11} = Z_{11}/Z_{21} & T_{12} = (Z_{11}Z_{22})/Z_{21} - Z_{12} \\ T_{21} = 1/Z_{21} & T_{22} = Z_{22}/Z_{21} \end{bmatrix} \quad (23)$$

Power cables are passive and symmetrical sub-systems, which means simplifications can be done in $\boldsymbol{Z}$ matrix :

$$Z_{22} = Z_{11} \qquad Z_{21} = Z_{12} \quad (24)$$

The coefficients of cables $\boldsymbol{Z}$ matrix (25) are obtained accordingly to the circuit simplification, shown in Fig. 14.

$$Z_{11} = \left(\frac{r(\omega)}{2} + j\omega\frac{l(\omega)}{2}\right)\Delta z + \frac{1}{(j\omega.c(\omega) + g(\omega)).\Delta z}$$
$$Z_{12} = \frac{1}{(j\omega.c(\omega) + g(w)).\Delta z} \quad (25)$$

Sub-systems association is facilitated. Cascading two port networks allows fast simulations and cables parametric studies. To build different length cable models, we consider the equivalent matrix $\boldsymbol{T_{eq}}$ of the series connection of n identical two port networks. This matrix is obtained simply by carrying out the matrix multiplication as follow:

$$T_{eq} = \prod_{i=1}^{n} T_i = T^n \quad (26)$$

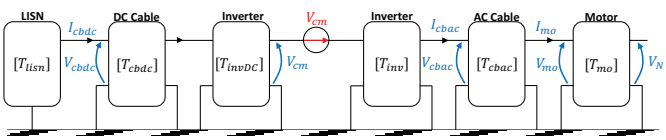

Fig. 13. Common mode quadripolar model

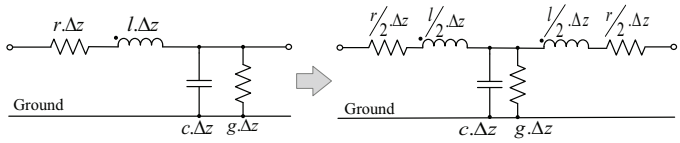

Fig. 14. T equivalent per-unit-length circuit of transmissions lines equations

This mathematical approach allows to take account of the frequency dependency of each matrix, easily. Results are obtained in less than 300 ms and shown in Fig. 15. As expected, the association of long cables and the electric motor generate resonances which are excited by the inverter fast commutations. Such resonances led to higher CM currents levels

VII. Conculsion

The use of unshielded cable models in conducted EMI simulations was investigated in this paper. As we previously mentioned, the models can be used to perform other simulations, making it possible to reduce output overvoltages at the motor terminals. Moreover, the developed predictive models can be easily integrated in conducted emissions simulations. The proposed approach lead to perform fast CM currents evaluations. For future means of transportation, it is necessary to optimize electromechanical chain by taking into account multi-constraints ageing and conducted disturbances up to 100 MHz. New design guidelines will be provided in future works with the objective of optimizing the mass and losses of EMI filters at operating system level.

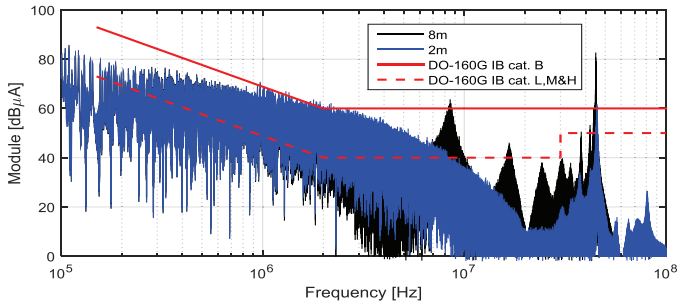

Fig. 15. CM currents at inverters output (F_{sw} = *15 kHz, Iout = 20A*)

References

[1] RTCA (2014), Environmental Conditions and Test Procedures for Airborne Equipment, DO160-G, Section 21, 2014.

[2] C.R. Paul, "Analysis of multiconductor transmission lines." John Wiley & Sons, 2008.

[3] D. WESTON. "Electromagnetic Compatibility: Principles and Applications, Revised and Expanded". CRC Press, 2001.

[4] M. S. Raven. "Experimental measurements of the skin effect and internal inductance at low frequencies". *Acta Techn*, 2015, vol. 60, p. 51-69.

[5] N. Idir, Y. Weens, JJ. Franchaud. "Skin effect and dielectric loss models of power cables". *IEEE Transactions on Dielectrics and Electrical Insulation*, 2009, vol. 16, no 1, p. 147-154.

[6] D. Meeker. "Finite Element Method Magnetics (FEMM)"

[7] B. Revol, F. Adam, C. Gautier, F. Costa "Modèle générique de cables de puissance: une première approche vers une modélisation système"

[8] V. Dos Santos, B. Cougo, N. Roux, B. Sareni, B. Revol, JP. Carayon. "Trade-off between Losses and EMI Issues in Three-Phase SiC Inverters for Aircraft Applications". *(Accepted to EMC 2017 international conference, Washington DC, USA)*.